A general conversion of polyacrylate–metal complexes into porous carbons especially evinced in the case of magnesium polyacrylate†

Xiang Ying Chen,*[a] Chong Chen,[a] Zhong Jie Zhang,[b] Dong Hua Xie[a] and Jian Wei Liu[c]

As a generalized synthetic protocol, porous carbons have been for the first time prepared by a direct carbonization of polyacrylate–metal complexes. The case of magnesium polyacrylate was emphatically studied. It reveals that the carbonization temperature can play a crucial role in the determination of surface areas, pore structures, surface functionalities of porous carbons as well as the correlative capacitive performances. The **carbon-Mg-900** sample exhibits a high surface area of 942 m^2 g^{-1} and a large total pore volume of 1.90 cm^3 g^{-1}, with a high specific capacitance of 262.4 F g^{-1} at 0.5 A g^{-1} in 6.0 mol L^{-1} aqueous KOH electrolyte. Moreover, it displays high capacitance retention even of 33.5% at 100 A g^{-1}, and long-term cycling ability (∼91.3% retention after 5000 cycles). More importantly, the present synthetic strategy can be extended to prepare other polyacrylate–metal complexes, such as calcium polyacrylate and aluminum polyacrylate. The **carbon-Al-900** sample can exhibit a high surface area of 1556 m^2 g^{-1} and a large total pore volume of 0.97 cm^3 g^{-1}. To sum up, the carbon samples derived from magnesium polyacrylate possess the highest capacitive performances as supercapacitor electrode materials.

1 Introduction

Highly porous carbon has attracted great attention because of its low density, high specific surface area, tunable porous structure, high thermal conductivity, good electrical conductivity, mechanical stability and mass productivity,[1] which can result in prospective applications in the fields of catalyst, catalyst support, absorbent, hydrogen storage and electrochemical energy storage.[2] To tackle the energy and environmental problems nowadays, supercapacitors based on porous carbon materials have been applied considerably, which can bridge the gap between batteries and conventional dielectric capacitors, and are ideal for the rapid storage and release of energy.[3,4]

Porous carbons are usually obtained *via* carbonization of natural or synthetic precursors, followed by activation. To circumvent the disadvantages incurred by chemical/physical activation treatments, a direct carbonization method has been currently developed to prepare porous carbon. For example, Yamauchi *et al.* reported the synthesis of nanoporous carbon by direct carbonization of Al-based porous coordination polymers[5] or zeolitic imidazolate framework (ZIF-8).[6] On the other hand, two types of templates, classified as hard template or soft template, have been thus far used as scaffolds to achieve porous materials.[7] As far as hard template is concerned, it can offer rigid nanocast molds to replicate carbon materials, controllably producing porous structures. Excellent examples include nanoporous carbons prepared by Inagaki *et al.* by direct carbonization of a mixture of MgO, serving as a hard template, and a thermoplastic precursor.[8]

A metal complex (also known as coordination polymer), consisting of an atom or ion (usually metallic) and a surrounding array of bound molecules or anions, displays the shape-selective, predictable, topological architectures together with the homogeneous metal dispersion,[9] which is an alternative candidate for porous carbon synthesis. Apart from the above-mentioned porous carbon synthesis method of Yamauchi, other kinds of metal complex were also reported for porous carbon synthesis, including zinc glycolate,[10] Zn-based MOFs,[11,12] IRMOF-1/3/8 [13] and tris(functionalised-phenylethynyl)benzene–metal complexes.[14] Hence, further exploring metal complexes for the synthesis of porous carbon together with their application in supercapacitors is of great importance.

[a]*School of Chemical Engineering, Anhui Key Laboratory of Controllable Chemistry Reaction & Material Chemical Engineering, Hefei University of Technology, Hefei, Anhui 230009, P. R. China. E-mail: cxyhfut@gmail.com; Fax: +86-551-2901450; Tel: +86-551-2901450*

[b]*College of Chemistry & Chemical Engineering, Anhui Province Key Laboratory of Environment-friendly Polymer Materials, Anhui University, Hefei 230039, Anhui, P. R. China. E-mail: zhangzj0603@126.com*

[c]*Department of Physics and Astronomy, University of Kansas, Lawrence, KS 66045, USA. E-mail: liuw@ku.edu; Fax: +1-785-8645264; Tel: +1-785-8642274*

† Electronic supplementary information (ESI) available. See DOI: 10.1039/c3ta01330h

This journal is © The Royal Society of Chemistry 2013

J. Mater. Chem. A, 2013, **1**, 4017–4025 | **4017**

On the other hand, sodium polyacrylate, also known as waterlock, is a polymer with the chemical formula [–CH$_2$–CH(COONa)–]$_n$ widely used in consumer products. It is famous for its extraordinary water absorbing ability, which can hold 800 times its weight of water. Therefore it has a wide range of applications from baby diaper to contact lens.[15,16] More importantly, polyacrylate ions can coordinate with Mg^{2+} ions with an ideal molar ratio of 2 : 1 to form an insoluble magnesium polyacrylate complex,[17] which probably serves as the precursor for porous carbon synthesis by the direct carbonization method.

Herein, we present a straightforward carbonization method to prepare porous carbon without further physical/chemical activation, using magnesium polyacrylate complex as the precursor. The specific surface areas, pore structures, and capacitive performances of the as-obtained porous carbons are well investigated. More interestingly, the present synthetic method can be extended to the synthesis of calcium polyacrylate complex and aluminum polyacrylate complex, which are further converted into porous carbons after the carbonization process.

2 Experimental

All analytical chemicals were purchased from Sinopharm Chemical Reagent (Shanghai) Co. Ltd, and were used as received without further treatment.

When sodium polyacrylate comes in contact with water, Na$^+$ detaches itself, leaving negatively charged chains of carboxyl ions, which unwind to form a 3D structure as it absorbs water. These carboxyl ions can coordinate with Mg^{2+} ions to produce a magnesium polyacrylate complex, whose chain-like structures will curl after the air drying process (step 1). The complex was then carbonized to form the composites containing amorphous carbon and magnesium oxides (step 2). After washing with dilute HCl solution and deionized water, magnesium oxides were removed and only porous carbon was left, named as **carbon-Mg-700/800/900** for convenient referencing (step 3). Finally, structure characterization and capacitive measurements were performed on the as-obtained carbon. The panoramic schematic route is depicted in Fig. 1.

2.1 Typical room temperature synthetic procedure for the magnesium polyacrylate complex

Mg(OAc)$_2$·4H$_2$O and sodium polyacrylate (molar ratio of 1 : 2) pre-dissolved in deionized water were mixed together under constant magnetic stirring for 4 h at room temperature, resulting in the formation of a white magnesium polyacrylate complex. Then, the precipitate was filtered off, washed with deionized water and absolute ethanol several times, and then dried in air at 120 °C for 12 h.

2.2 Typical direct carbonization synthetic procedure for carbon sample

The above-prepared magnesium polyacrylate powder was first ground, and then placed in a porcelain boat, flushing with Ar flow for 30 min, and further heated in a horizontal tube furnace up to 700/800/900 °C at a rate of 5 °C min^{-1} and maintained at
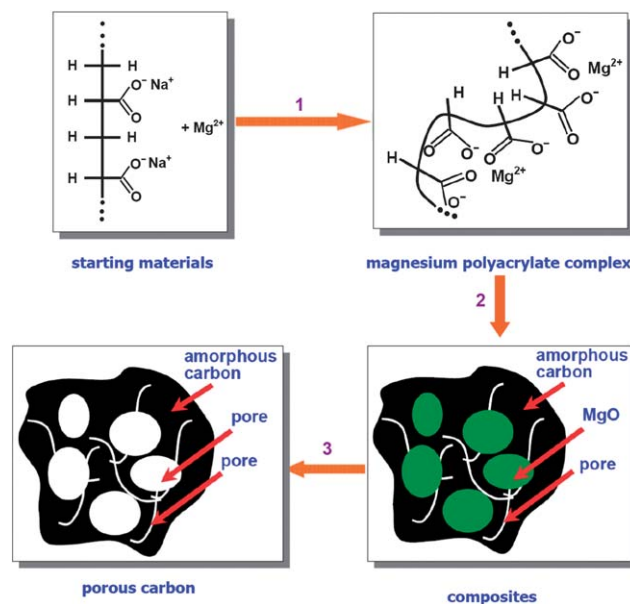

Fig. 1 Schematic route showing the production of porous carbon by heating the magnesium polyacrylate complex at the carbonization temperatures of 700/800/900 °C.
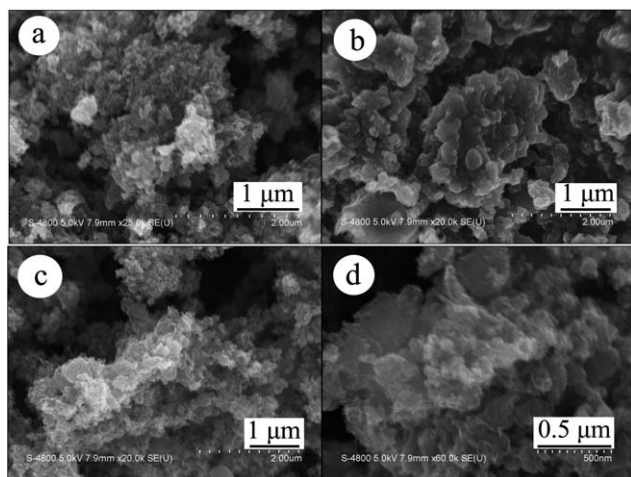
this temperature for 2 h under Ar flow. The resultant product was immersed in dilute HCl solution to remove soluble/insoluble substances, and subsequently washed with adequate deionized water. Finally, the sample was dried under vacuum at 120 °C for 12 h to obtain the **carbon-Mg-700/800/900** samples.

2.3 Characterization

X-ray diffraction (XRD) patterns were obtained on a Rigaku D/MAX2500V with Cu Kα radiation. Field emission scanning electron microscopy (FESEM) images were taken with a Hitachi S-4800 scanning electron microscope. X-ray photoelectron
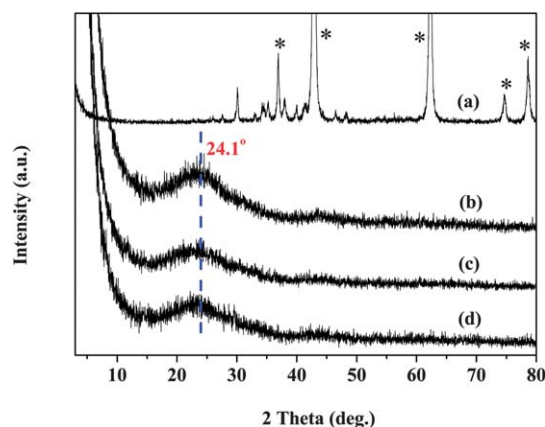
Fig. 2 XRD patterns: (a) **carbon-Mg-800** sample before being washed with aqueous HCl solution and deionized water; (b) **carbon-Mg-700**, (c) **carbon-Mg-800** and (d) **carbon-Mg-900** samples after being washed with aqueous HCl solution and deionized water to remove any unwanted impurities. Notes: * = cubic MgO (JCPDS card no. 45-0946).

4018 | *J. Mater. Chem. A*, 2013, **1**, 4017–4025

This journal is © The Royal Society of Chemistry 2013

**Fig. 3** FESEM images of the carbons: (a) **carbon-Mg-700**, (b) **carbon-Mg-800** and (c and d) **carbon-Mg-900**.

spectra (XPS) were obtained on a VGESCALAB MK II X-ray photoelectron spectrometer with an exciting source of Mg Kα (1253.6 eV). The specific surface area and pore structure of the carbon samples were determined by N_2 adsorption–desorption isotherms at 77 K (Quantachrome Autosorb-iQ) after being vacuum-dried at 150 °C overnight. The specific surface areas were calculated by the BET (Brunauer–Emmett–Teller) method. Cumulative pore volume and pore-size distribution were calculated using a slit/cylindrical nonlocal density functional theory (NLDFT) model.

2.4 Electrochemical measurements

In order to evaluate the capacitive performances of the as-prepared carbon samples (∼4 mg) in electrochemical capacitors, a mixture of 80 wt% of the carbon sample, 15 wt% of acetylene black and 5 wt% of polytetrafluoroethylene (PTFE) binder was fabricated using ethanol as a solvent. A slurry of the above mixture was subsequently pressed onto nickel foam under a pressure of 20 MPa, serving as the current collector. The prepared electrode was placed in a vacuum drying oven at 120 °C for 24 h. A three electrode experimental setup taking a 6.0 mol L^{-1} KOH aqueous solution as the electrolyte was used in cyclic voltammetry and galvanostatic charge–discharge measurements on an electrochemical working station (CHI660D, ChenHua Instruments Co. Ltd., Shanghai). Here, the prepared electrode, platinum foil (6 cm^2) and saturated calomel electrode (SCE) were used as the working, counter and reference electrodes, respectively.

3   Results and discussion

The component, crystallinity and purity of the carbon samples were studied using the XRD technique. On heating magnesium polyacrylate, acting as a carbon precursor, at 800 °C for 2 h under Ar flow, a large amount of light black powder appears. It is composed of amorphous carbon, cubic MgO (JCPDS card no. 45-0946) together with minor unidentified substances, whose XRD pattern is shown in Fig. 2a. The occurrence of MgO well complies with the previous results concerning the sol–gel production of MgO fibers by heating magnesium polyacrylate at
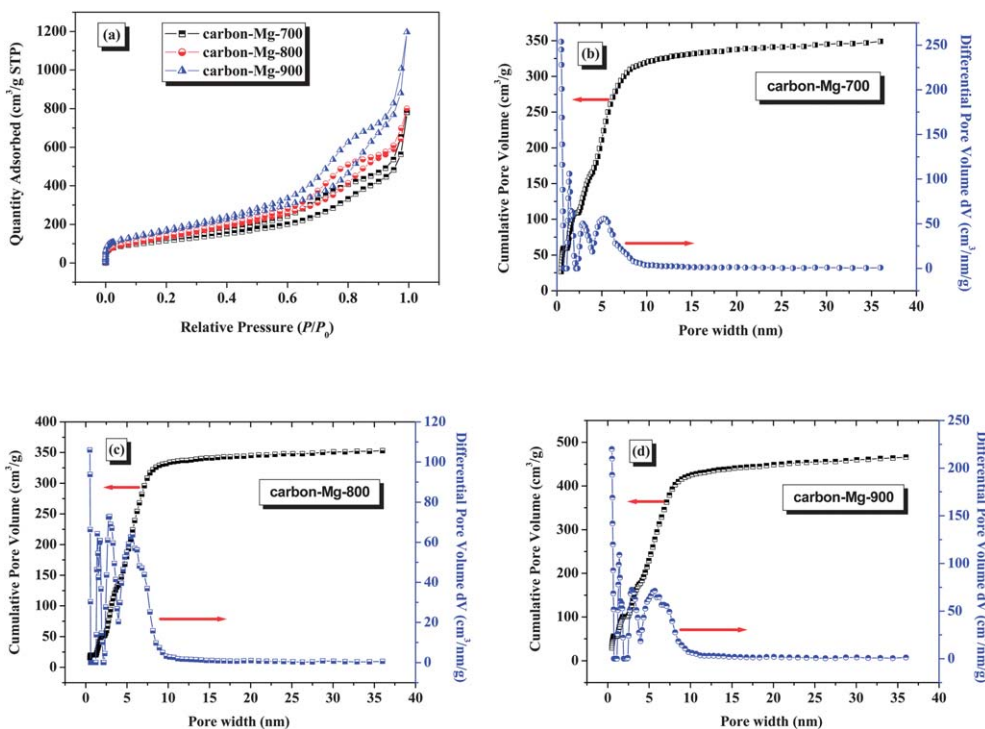
Fig. 4 (a) N_2 adsorption–desorption isotherms and (b–d) cumulative pore volume and pore-size distribution (calculated using a slit/cylindrical NLDFT model).

600 °C.[18] After being washed with aqueous HCl solution and deionized water to remove any unwanted impurities, the deep black **carbon-Mg-800** sample is engendered, as given in Fig. 2c. The diffraction peaks located at *ca.* 24.1 are ascribed to the (002) plane of graphite. Meanwhile, the **carbon-Mg-700/900** samples display similar XRD results to that of the **carbon-Mg-800** sample. Furthermore, the broad and low densities of XRD patterns in Fig. 2 clearly reveal the amorphous or low crystallinity features of present carbons.[19]

The genuine shape and size of the carbon samples were investigated using the FESEM technique. Fig. 3a shows the representative FESEM image of the **carbon-Mg-700** sample, which is made up of a large quantity of nanoscale carbon particles. The **carbon-Mg-800/900** samples, as depicted in Fig. 3b–d, demonstrate the analogous shapes and sizes to that of the **carbon-Mg-700** sample. Besides, considering the self-carbonization and/or collapse of polyacrylate chains of the metal complex as well as the templating effect of MgO at elevated temperatures, nanoporous structures are expected to occur within the carbon products.

The Brunauer–Emmett–Teller (BET) surface areas and pore structures of the **carbon-Mg-700/800/900** samples were calculated by N_2 adsorption–desorption isotherms and pore size distributions were calculated using a slit/cylindrical NLDFT model. All isotherms in Fig. 4a are type IV according to IUPAC classification, unexceptionally evincing the existence of multiple pore sizes ranging from micropores to macropores.[20] A small amount of nitrogen adsorption at a low relative pressure (<0.45 P/P_0) indicates that their microporosities are not so high. The hysteresis at a medium relative pressure (0.45–1.0 P/P_0) reveals capillary condensation in predominant mesopores and vertical tails existing at a high pressure (~1.0 P/P_0) imply the presence of macroporosity.[21,22] To more precisely characterize the pore size distribution, especially in microscale scope below 2 nm, a hybrid nonlocal DFT (NLDFT) kernel from nitrogen adsorption was applied. It assumes a slit pore geometry for micropores and a cylindrical pore geometry for mesopores. The resultant cumulative pore volumes and pore size analysis of the **carbon-Mg-700/800/900** samples are given in Fig. 4b–d, further revealing multi-modal pore structures expressly in the scope of 0.5–10 nm.

All specific surface areas and pore structures of the **carbon-Mg-700/800/900** samples are listed in Table 1. By applying the appropriate carbonization temperature, both high surface areas

and large pore volumes are realized. The BET surface areas are of 862–1051 m^2 g^{-1} while the total pore volumes range from 1.53 to 1.93 cm^3 g^{-1}.

The empirical composition, functional groups, chemical state and electronic state of the elements of the carbons were determined using the XPS technique, providing a compositional estimate of only the outermost layers, with a penetration depth of *ca.* 5–15 nm.[23,24] Fig. 5a shows the survey spectra of the **carbon-Mg-700/800/900** samples with binding energies ranging
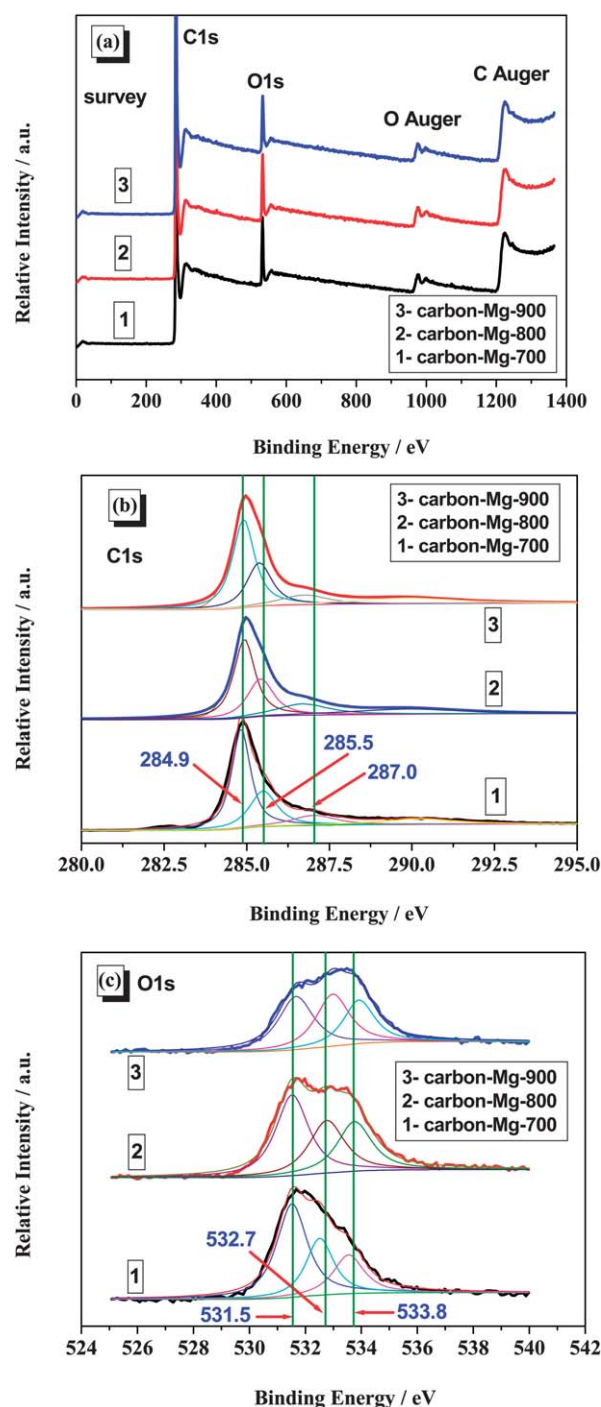

Fig. 5 XPS spectra of the carbon samples: (a) survey, (b) C1s, and (c) O1s.

Table 1 Characteristic surface areas and pore structures of the carbon samples[ab]

Sample	BET surface area (m^2 g^{-1})			Total pore volume (cm^3 g^{-1})	Average pore width (nm)
	Total	S_{micro}	S_{ext}		
Carbon-Mg-700	862	137	725	1.53	7.1
Carbon-Mg-800	1051	148	903	1.93	7.4
Carbon-Mg-900	942	144	798	1.90	8.0

[a] S_{micro} represents the micropore area calculated by the *t*-plot. [b] S_{ext} represents the external surface area calculated by the *t*-plot.

4020 | *J. Mater. Chem. A*, 2013, **1**, 4017–4025

This journal is © The Royal Society of Chemistry 2013

Table 2 XPS peak analysis of the carbon samples

Sample	C (at.%)	O (at.%)
Carbon-Mg-700	91.22	8.78
Carbon-Mg-800	92.10	7.90
Carbon-Mg-900	92.59	7.41

from 0 to 1400.0 eV. Clearly, all carbon samples exclusively are comprised of carbon and oxygen elements without any other impurities. By high resolution XPS analysis, C1s can principally be fitted into three peaks in the range of 280.0–295.0 eV, as illustrated in Fig. 5b. The peak centered at *ca.* 284.9 eV is due to the sp^2 C=C bond, while the one at *ca.* 285.5 eV can be attributed to the sp^3 C–C bond, genuinely proving the graphitic structure.[25] Regarding the peak located at *ca.* 287.0 eV, it is due to the C–O bond.[26]

On the other hand, Fig. 5c indicates the high resolution O1s spectra (525.0–540.0 eV), which can approximately be fitted into three peaks. The peak at *ca.* 531.5 eV can be assigned to the C=O bond. The peaks at *ca.* 532.7 eV owe to C–O or O–H or bound water, while the peak at *ca.* 533.8 eV is due to O–C–O chemical binding.[27,28] Finally, the contents of carbon and oxygen elements are summarized in Table 2. It is apparent that a higher carbonization temperature favors a higher carbon content accompanied by a lower oxygen content. The trends in Table 2 accord well with those of the C1s/O1s intensity peaks shown in Fig. 5a.

To estimate the capacitive properties of the **carbon-Mg-700/800/900** samples as supercapacitor electrodes, we first carried out cyclic voltammetry (CV) measurements at various potential scan rates from 10 to 400 mV s^{-1}. In the case of 10 mV s^{-1}, as shown in Fig. 6a, all samples exhibit nearly rectangular shapes in a potential range of −1.0 to 0 V, proving good double layer capacitive performance. Meanwhile, no obvious redox humps appear in these CV curves, an indication of no pseudo-capacitance involved or very little contribution from redox reaction.[29] From the viewpoint of CV integral areas, the present samples possess a similar specific capacitance at a low scan rate in that the integral area of the CV curve is proportional to the capacitance of the supercapacitor.[30] On further increasing the potential scan rate up to 50 mV s^{-1}, the resulting CV curves shown in Fig. 6b almost have the same shapes as those at 10 mV s^{-1}. However, in the case of 200/400 mV s^{-1}, the CV curves become apparently distorted in shapes, deviating far from ideal rectangles for supercapacitors.

As far as supercapacitor is concerned, the capacitance of the electrodes is proportional to the electrode–electrolyte interface, *i.e.* to the electrochemically available electrode surface area in electrolytic medium. In detail, the micropores play an essential role for ion adsorption and/or energy storage whereas large pores provide fast mass-transport of electrolytes to and out of the micropores.[31] The present **carbon-Mg-900** sample displaying the largest specific capacitance at a high scan rate is probably due to its high specific surface area and well-balanced micro/mesoporosity.
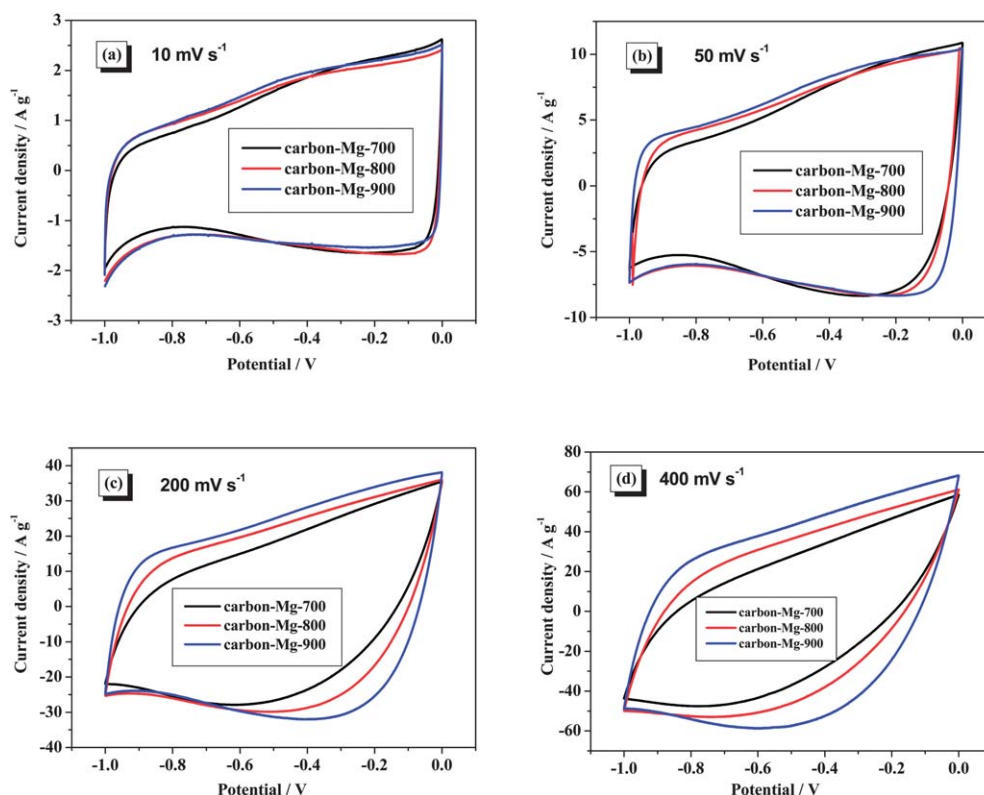
Fig. 6 Cyclic voltammograms of the **carbon-Mg-700/800/900** samples at various scan rates: (a) 10 mV s^{-1}, (b) 50 mV s^{-1}, (c) 200 mV s^{-1}, and (d) 400 mV s^{-1}.

This journal is © The Royal Society of Chemistry 2013

J. Mater. Chem. A, 2013, **1**, 4017–4025 | **4021**

Galvanostatic charge–discharge curves of the **carbon-Mg-700/800/900** samples were further measured at a current density of 10 A g^{-1} in 6.0 mol L^{-1} KOH aqueous solution, as displayed in Fig. 7a. All curves exhibit nearly symmetric triangular shapes in a potential range of −1.0 to 0 V using a typical three-electrode cell system. It confirms a good capacitive behavior and good charge propagation throughout the carbon material.

Next, the specific capacitances of active electrode materials are calculated according to the following equation:

$$C_m = \frac{I \times t}{\Delta V \times m}$$

where C_m (F g^{-1}) is the specific capacitance of the electrode based on the mass of active materials; I (A) is the discharge current; t (s) is the discharge time; ΔV (V) is the potential window (in the present work, $\Delta V = 1.0$ V); and m (mg) is the mass of active materials loaded in the working electrode.

Consequently, specific capacitances of these carbon samples at various current densities (0.5–100 A g^{-1}) are depicted in Fig. 7b. In detail, the **carbon-Mg-700/800** samples demonstrate specific capacitances of *ca.* 209.5 and 195.4 F g^{-1} at a current density of 0.5 A g^{-1}, respectively. Especially, the **carbon-Mg-900** sample displays the incredibly highest specific capacitance of 262.4 F g^{-1} at 0.5 A g^{-1}. The present specific capacitances are much higher than many results reported previously, such as mesoporous carbons derived from the citrates.[32] Along with the increase of current density,

the corresponding specific capacitance gradually decreases. The capacitance retention at a designated current density is also marked in Fig. 7b. Outstandingly, capacitance retention of the **carbon-Mg-900** sample can reach up to *ca.* 33.5% even at a high current density of 100 A g^{-1}, suggesting its good rate capability.

Long-term cycling stability of supercapacitors is an imperative factor for their practical applications.[33] Cycling stability of the **carbon-Mg-900** sample is demonstrated in Fig. 7c, showing the specific capacitance as a function of cycle number. Within the initial run of *ca.* 1000 cycles, the corresponding specific capacitance slowly deteriorates, while it tends to be almost invariable beyond 1000 cycles. After carrying out the charge–discharge process for 5000 times, it can retain capacitance of *ca.* 91.3% in contrast to that of the initial one. The CV curves of the 1st and 5000th cycles are also depicted in Fig. 7c. Compared to the 1st CV curve, the 5000th one has approximately the same shape but small shrinkage in area. The good cycling stability of the **carbon-Mg-900** sample is probably ascribed to the small amount of oxygen groups on the carbon surfaces and the higher degree of crystalline order that renders materials more stable.[34]

Fig. 7d presents the galvanostatic charge–discharge curves of the 1st and 5000th cycles of the **carbon-Mg-900** sample at the current density of 10 A g^{-1}. Both charge–discharge curves maintain the nearly triangular shapes in a potential range of −1.0 to 0 V except that the discharging time after 5000th cycle
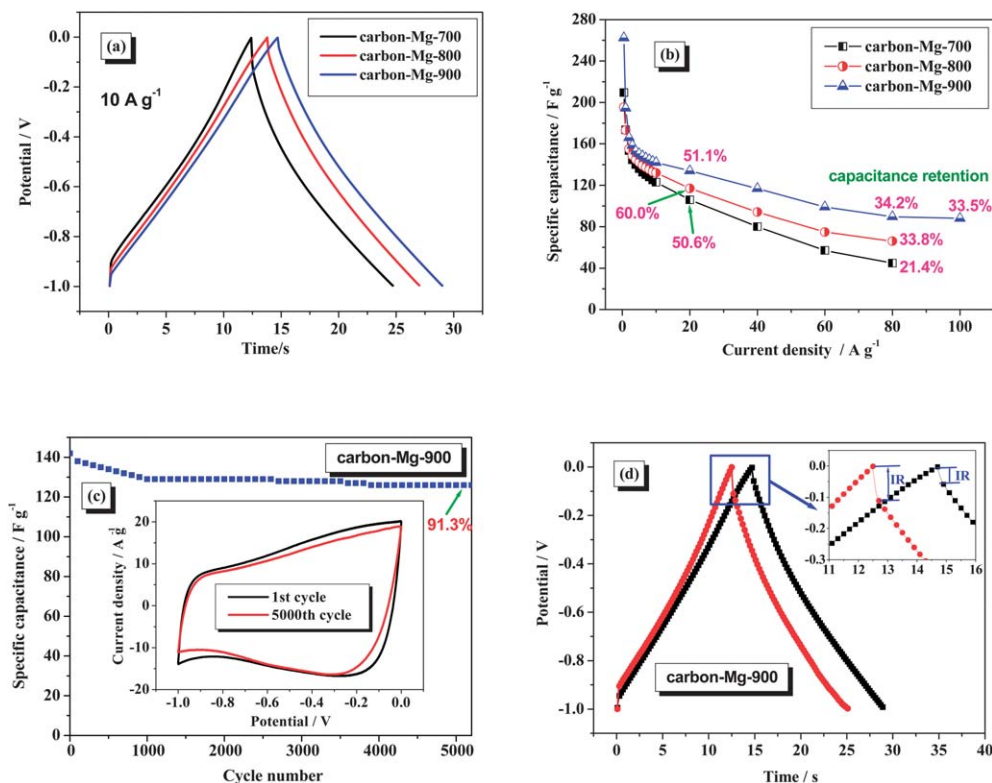
Fig. 7 (a) Galvanostatic charge–discharge curves measured at a current density of 10 A g^{-1} of the **carbon-Mg-700/800/900** samples; (b) specific capacitances at various current densities; (c) cycling stability of the **carbon-Mg-900** sample (the inset shows the CV curves of the 1st and 5000th cycles); (d) galvanostatic charge–discharge curves of the 1st and 5000th cycles of the **carbon-Mg-900** sample at the current density of 10 A g^{-1} (the inset shows the IR drops of the 1st and 5000th cycles).

has slightly shortened. Furthermore, the IR drop becomes gently larger after cycling for 5000 times, revealing the increase of overall internal resistance of the electrode.[35]

3.1 The generality of the present synthetic method

To validate the generality of the present synthetic method for producing porous carbons by a direct carbonization of poly-acrylate–metal complexes, we chose calcium polyacrylate and aluminum polyacrylate as the extension examples. It was found that calcining calcium polyacrylate to obtain a black product only happens at 700 °C for 2 h under Ar flow, named as **carbon-Ca-700**, and no solid product appears in cases of 800/900 °C. In contrast, black powders are produced by calcining aluminum polyacrylate at 700/800/900 °C with other reaction parameters unchanged, and the products are denoted as **carbon-Al-700/800/900**. The whole XRD patterns are displayed in Fig. 8. Similar to those shown in Fig. 2, the diffraction peak centering at *ca.* 24.5° can be indexed to the (002) plane of graphite. In addition, the broad and low-intensity peaks apparently indicate the amorphous structures within carbons.

Fig. 9a represents the typical FESEM image of the **carbon-Ca-700** sample. As depicted in the inset, it is totally composed of large numbers of pores of several hundreds of micrometers in size. The **carbon-Al-700** sample consists of floccular structures in abundance, as shown in Fig. 9b. As for **carbon-Al-800/900** samples, they are made up of a large number of irregular particles without any visible pores on the surfaces, as demonstrated in Fig. 9c and d.

Fig. 10a and b show CV curves of **carbon-Ca-700** and **carbon-Al-700/800/900** samples at scan rates of 10 and 100 mV s⁻¹. From the viewpoint of CV shape, the **carbon-Ca-700** sample is more close to ideal rectangle while the **carbon-Al-700/800/900** samples are very far from ideal rectangles, evincing good double layer performance of the **carbon-Ca-700** sample. Based on the CV areas, the order of specific capacitances is as follows: **carbon-Ca-700** > **carbon-Al-900** > **carbon-Al-800** > **carbon-Al-700**. Fig. 10c gives us the galvanostatic charge–discharge curves
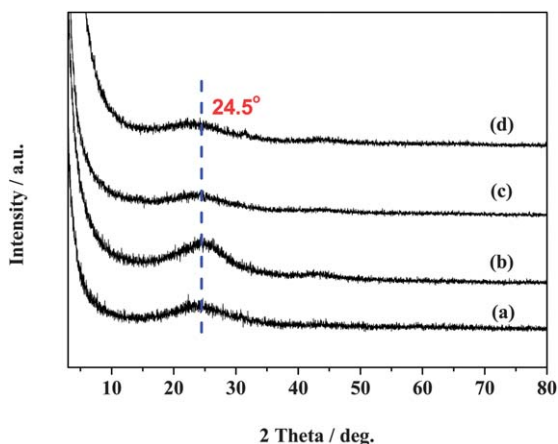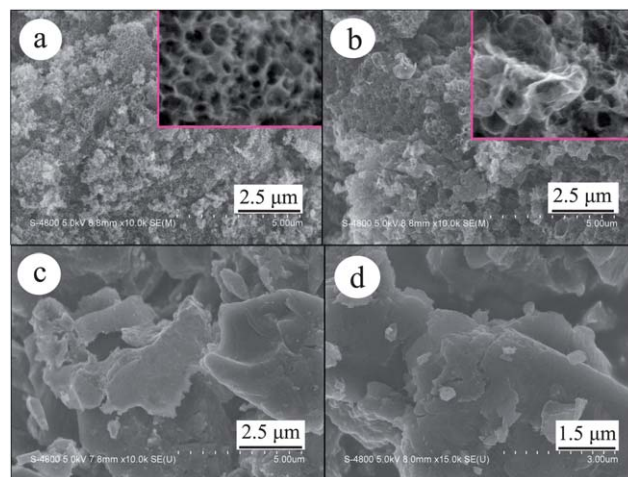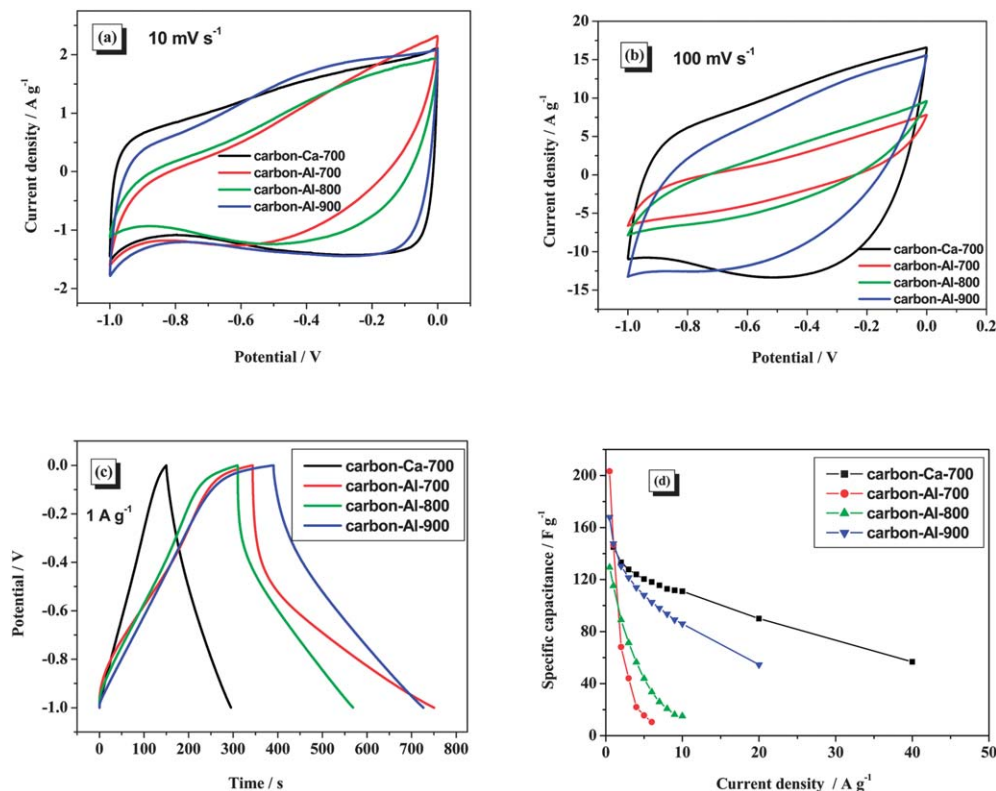

Fig. 9 FESEM images of the carbon samples: (a) **carbon-Ca-700**; (b) **carbon-Al-700**; (c) **carbon-Al-800** and (d) **carbon-Al-900**.

measured at the current density of 1 A g⁻¹, in which the **carbon-Ca-700** sample displays the best double layer performance due to its nearly symmetric triangles. Specific capacitances at various current densities are shown in Fig. 10d, in which the values are much lower than those of the **carbon-Mg-700/800/900** samples, as depicted in Fig. 7b.

Considering the relatively high rate capabilities of the **carbon-Ca-700** and **carbon-Al-900** samples, we further studied their surface areas and pore structures. N₂ adsorption–desorption isotherms in Fig. 11a reveal that the **carbon-Ca-700** sample exhibits a type IV isotherm according to IUPAC, with a certain amount of micro-/meso-/macropores coexistent within carbon. From the viewpoint of isotherm shape, it is conferred that large pores including mesopores and macropores are predominant within the **carbon-Ca-700** sample. On the other hand, as seen in Fig. 11b, the **carbon-Al-900** sample exhibits a type I isotherm, with significant adsorption below relative pressure $P/P_0 < 0.3$, due to the capillary filling of micropores. The isotherms also exhibit some nitrogen uptake as a kind of hysteresis at $0.3 < P/P_0 < 1.0$, which may be attributed to adsorption into meso-/macropores arising from interparticle voids.[36] By all appearances, the existence of micropores is predominating within the **carbon-Al-900** sample based on the analysis of the isotherm in Fig. 11b.

The whole surface areas and pore structures of the carbon samples are listed in Table 3. The **carbon-Ca-700** sample indicates a surface area of 285 m² g⁻¹ and a total pore volume of 0.57 cm³ g⁻¹, which are much lower than those of the **carbon-Mg-700/800/900** samples. Interestingly, the **carbon-Al-900** sample exhibits a high surface area of 1556 m² g⁻¹ and a large total pore volume of 0.97 cm³ g⁻¹ compared with those of the **carbon-Ca-700** sample. From the results in Fig. 10, 11 and Table 2, we can conclude that the electrochemical performance of carbon is not proportional to its surface area and total pore volume. No matter what, the **carbon-Al-900** sample having a high surface area and large porosity is expected for applications as absorbent, catalyst support, *etc.*

Fig. 8 XRD patterns of the carbon samples: (a) **carbon-Ca-700**; (b) **carbon-Al-700**; (c) **carbon-Al-800** and (d) **carbon-Al-900**.

Fig. 10 Cyclic voltammograms at scan rates: (a) 10 mV s^{-1} and (b) 100 mV s^{-1}; (c) galvanostatic charge–discharge curves measured at the current density of 1 A g^{-1}; (d) specific capacitances at various current densities of the **carbon-Ca-700** and **carbon-Al-700/800/900** samples.
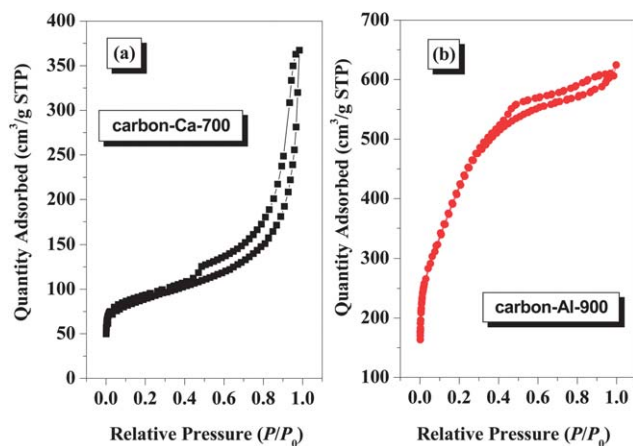
Fig. 11 N$_2$ adsorption–desorption isotherms of the **carbon–Ca-700/carbon–Al-900** samples.

Table 3 Characteristic surface areas and pore structures of the carbon samples[ab]

Sample	BET surface area (m^2 g^{-1})			Total pore volume (cm^3 g^{-1})	Average pore width (nm)
	Total	S_{micro}	S_{ext}		
Carbon–Ca-700	285	125	160	0.57	8.0
Carbon–Al-900	1556	812	744	0.97	2.5

[a] S_{micro} represents the micropore area calculated by the *t*-plot. [b] S_{ext} represents the external surface area calculated by the *t*-plot.

4 Conclusions

We demonstrate a simple but effective carbonization method to prepare porous carbons using polyacrylate–metal complexes as precursors. The impact of carbonization temperature upon surface areas, pore structures, surface functionalities of porous carbons as well as the resulting capacitive performances was primarily investigated. We believe that several scientific advantages exist in the present work: (1) the direct carbonization method is convenient and simple for preparing porous carbons, without any physical/chemical activation process; (2) the sodium polyacrylate used is inexpensive and commercially available, revealing economic potentials for practical applications in large scale; (3) the porous carbons derived from polyacrylate–metal complexes display high surface areas, large pore volumes as well as the correlative capacitive behaviors; (4) the polyacrylate–metal complexes can be extended to other kinds of metal ions such as Zn^{2+}, Mn^{2+}, Fe^{3+}, *etc.*

Acknowledgements

References

1 A. Stein, Z. Wang and M. A. Fierke, *Adv. Mater.*, 2009, **21**, 265.

2 H. Nishihara and T. Kyotani, *Adv. Mater.*, 2012, **24**, 4473.

3 P. Simon and Y. Gogotsi, *Nat. Mater.*, 2008, **7**, 845.

4 L. L. Zhang and X. S. Zhao, *Chem. Soc. Rev.*, 2009, **38**, 2520.

5 M. Hu, J. Reboul, S. Furukawa, N. L. Torad, Q. Ji, P. Srinivasu, K. Ariga, S. Kitagawa and Y. Yamauchi, *J. Am. Chem. Soc.*, 2012, **134**, 2864.

6 W. Chaikittisilp, M. Hu, H. Wang, H. S. Huang, T. Fujita, K. C. W. Wu, L. C. Chen, Y. Yamauchi and K. Ariga, *Chem. Commun.*, 2012, **48**, 7259.

7 Y. D. Xia, Z. X. Yang and R. Mokaya, *Nanoscale*, 2010, **2**, 639.

8 T. Morishita, T. Tsumura, M. Toyoda, J. Przepiórski, A. W. Morawski, H. Konno and M. Inagaki, *Carbon*, 2010, **48**, 2690.

9 M. O'Keeffe and O. M. Yaghi, *Chem. Rev.*, 2012, **112**, 675.

10 W. Li, F. Zhang, Y. Dou, Z. Wu, H. Liu, X. Qian, D. Gu, Y. Xia, B. Tu and D. Zhao, *Adv. Energy Mater.*, 2011, **1**, 382.

11 B. Liu, H. Shioyama, T. Akita and Q. Xu, *J. Am. Chem. Soc.*, 2008, **130**, 5390.

12 H. L. Liang, B. Liu, Y. Q. Lan, K. Kuratani, T. Akita, H. Shioyama, F. Zong and Q. Xu, *J. Am. Chem. Soc.*, 2011, **133**, 11854.

13 S. J. Yang, T. Kim, J. H. Im, Y. S. Kim, K. Lee, H. Jung and C. R. Park, *Chem. Mater.*, 2012, **24**, 464.

14 N. Kobayashi and M. Kijima, *J. Mater. Chem.*, 2008, **18**, 1037.

15 R. Schweins and K. Huber, *Eur. Phys. J. E: Soft Matter Biol. Phys.*, 2001, **5**, 117.

16 Y. Hu, J. Beach, J. Raymer and M. Gardner, *J. Exposure Anal. Environ. Epidemiol.*, 2004, **14**, 378.

17 C. De Stefano, A. Gianguzza, D. Piazzese and S. Sammartano, *Talanta*, 2003, **61**, 181.

18 G. Kordas, *J. Mater. Chem.*, 2000, **10**, 1157.

19 L. Lu, V. Sahajwalla, C. Kong and D. Harris, *Carbon*, 2001, **39**, 1821.

20 S. Wei, H. Zhang, Y. Huang, W. Wang, Y. Xia and Z. Yu, *Energy Environ. Sci.*, 2011, **4**, 736.

21 S. W. Woo, K. Dokko, H. Nakano and K. Kanamura, *J. Mater. Chem.*, 2008, **18**, 1674.

22 D. W. Wang, F. Li and H. M. Cheng, *J. Power Sources*, 2008, **185**, 1563.

23 H. Darmstadt, C. Roy, S. Kaliaguine, S. J. Choi and R. Ryoo, *Carbon*, 2002, **40**, 2673.

24 J. L. Figueiredo, M. F. R. Pereira, M. M. A. Freitas and J. J. M. Órfão, *Carbon*, 1999, **37**, 1379.

25 T. I. T. Okpalugo, P. Papakonstantinou, H. Murphy, J. McLaughlin and N. M. D. Brown, *Carbon*, 2005, **43**, 153.

26 V. Datsyuk, M. Kalyva, K. Papagelis, J. Parthenios, D. Tasis, A. Siokou, I. Kallitsis and C. Galiotis, *Carbon*, 2008, **46**, 833.

27 G. D. B. Beamson, *High Resolution XPS of Organic Polymers*, Wiley, Chichester, 1992.

28 W. F. Yap, W. M. M. Yunus, Z. A. Talib and N. A. Yusof, *Int. J. Phys. Sci.*, 2011, **6**, 2744.

29 L. F. Chen, X. D. Zhang, H. W. Liang, M. G. Kong, Q. F. Guan, P. Chen, Z. Y. Wu and S. H. Yu, *ACS Nano*, 2012, **6**, 7092.

30 E. E. Kalu, T. T. Nwoga, V. Srinivasan and J. W. Weidner, *J. Power Sources*, 2001, **92**, 163.

31 C. Vix-Guterl, E. Frackowiak, K. Jurewicz, M. Friebe, J. Parmentier and F. Béguin, *Carbon*, 2005, **43**, 1293.

32 J. Zhou, X. Yuan, W. Xing, W. Si and S. Zhuo, *Carbon*, 2010, **48**, 2765.

33 T. Brousse, P. L. Taberna, O. Crosnier, R. Dugas, P. Guillemet, Y. Scudeller, Y. Zhou, F. Favier, D. Bélanger and P. Simon, *J. Power Sources*, 2007, **173**, 633.

34 V. Ruiz, C. Blanco, M. Granda and R. Santamaría, *Electrochim. Acta*, 2008, **54**, 305.

35 L. Zhang and G. Q. Shi, *J. Phys. Chem. C*, 2011, **115**, 17206.

36 Y. D. Xia, Y. Q. Zhu and Y. Tang, *Carbon*, 2012, **50**, 5543.

This journal is © The Royal Society of Chemistry 2013

J. Mater. Chem. A, 2013, **1**, 4017–4025 | **4025**